Chemical Engineering Journal 354 (2018) 93–104

Contents lists available at ScienceDirect

Chemical Engineering Journal

journal homepage: www.elsevier.com/locate/cej

Electrochemical oxidation of volatile organic compounds in all-solid cell at ambient temperature

Bo Zhang[a], Min Chen[a,b], Lian Wang[a], Xu Zhao[a,b], Renzhi Hu[b,c], Hao Chen[c], Pinhua Xie[b,c,d], Changbin Zhang[a,b,*], Hong He[a,b,d]

[a] State Key Joint Laboratory of Environment Simulation and Pollution Control, Research Center for Eco-Environmental Sciences, Chinese Academy of Sciences, Beijing 100085, China
[b] University of Chinese Academy of Sciences, Beijing 100049, China
[c] State Key Laboratory of Environmental Optics and Technology, Anhui Institute of Optics and Fine Mechanics, Chinese Academy of Sciences, Hefei 230031, China
[d] Center for Excellence in Regional Atmospheric Environment, Institute of Urban Environment, Chinese Academy of Sciences, Xiamen 361021, China

HIGHLIGHTS

- Electrooxidation of volatile organic compounds were performed in all-solid cell.
- Benzene toluene and o-xylene (BTX) were 100% conversion to CO_2 and CO (CO_2 yield > 85%).
- No gaseous organic byproducts were present in the electro-oxidation of BTX ($P_{cell} \geq 2.0$ V).
- Benzene oxidation process was mediated by·OH generated from water vapor discharge at $P_{cell} = 2.0$ V.
- Electrooxidation of BTX in all-solid cell is a promising method for applications in indoor air purification.

GRAPHICAL ABSTRACT

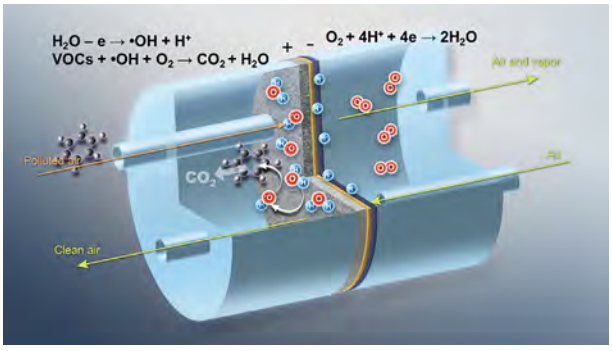

ARTICLE INFO

Keywords:
Volatile organic compounds
Electrocatalytic oxidation
Indoor air pollution
Hydroxyl radicals

ABSTRACT

The catalytic elimination of indoor low-concentration gaseous benzene, toluene and o-xylene (BTX) under ambient conditions remains a challenge. Here, we firstly report a facile gas-solid interface electrochemical oxidation method for the mineralization of BTX at ambient temperature. A membrane electrode assembly (MEA) was used in the all-solid cell. An antimony-doped SnO_2 catalyst was coated onto the surface of a porous Ti foam to act as the anode, and reduced graphene oxide/carbon fiber paper-supported Pt (Pt/rGO/CFP) was employed as the cathode. The activity test results showed that 100% BTX conversion to CO_2 (85–99%) and CO (15–1%) was achieved within 4–5 h at the optimal cell voltage of 2.0 V at relative humidity 60%. Proton-transfer-reaction time-of-flight mass spectrometry and Fourier transform infrared spectroscopy results showed that no organic byproducts could be detected in the anodic reservoir. ·OH generated from water vapor discharge was measured directly by laser-induced fluorescence techniques. The electrochemical behavior of the working electrode in benzene solutions with different concentrations revealed that the benzene oxidation process was mainly mediated by ·OH at the onset potential of OER (2.0 V vs Ag/AgCl, saturated KCl). Our findings provide evidence that the gas-solid interface electrochemical oxidation method can be a potential method for ambient VOC destruction in indoor air environments.

* Corresponding author at: State Key Joint Laboratory of Environment Simulation and Pollution Control, Research Center for Eco-Environmental Sciences, Chinese Academy of Sciences, Beijing 100085, China.
E-mail address: cbzhang@rcees.ac.cn (C. Zhang).

https://doi.org/10.1016/j.cej.2018.07.208
Received 2 May 2018; Received in revised form 17 July 2018; Accepted 30 July 2018
Available online 31 July 2018

1. Introduction

Volatile organic compounds (VOCs), emitted from various industrial and natural sources, are key precursors for the formation of haze in the atmosphere and also have high toxicity potential toward human beings. VOCs are also a major class of indoor air contaminants, mainly released from consumer household products, adhesives and building materials, furnishing materials and combustion processes, and so on [1–3]. The Environmental Protection Agency estimated that the VOC levels in indoor air are 5–10 times higher than those of outdoor air [4]. Many VOCs are toxic and have been reported to cause carcinogenic, mutagenic, and teratogenic effects in humans [5]. Human beings spend > 80% of their lifetime indoors, including in living and working spaces [6,7]. Hence, it is very important to eliminate indoor air VOCs to meet environmental regulations and health needs.

Numerous studies [8–12] have been conducted for the development of effective and convenient methods to mitigate indoor air pollution. Catalytic combustion is the most effective way to abate industrial VOC emissions since VOCs can be oxidized to CO_2 over certain catalysts. Unfortunately, since the catalytic oxidation of VOCs at ambient temperature has not been achieved to date, this approach has not been utilized for indoor VOC removal. Currently, adsorption, biofilters, photocatalysis and non-thermal plasma methods have efficiently achieved ambient VOC destruction; however, some problems such as low light efficiency, byproduct formation, and operational risk are encountered with these methods. Photoelectrocatalysis (PEC), an electrically enhanced photocatalysis method, has been carried out in room-temperature air treatments in recent years [13,14]. Up to now, only small organic molecules, including gas-phase ethanol and methanol, can be converted to CO_2, with low yield [13,14]. The mineralization of common intractable indoor air contaminants such as benzene, toluene and xylene (BTX) has not been investigated using an all-solid PEC. Therefore, it is highly desirable to develop a novel and efficient method appropriate for VOC elimination under indoor air conditions.

Electrochemical oxidation technologies have been considered as an alternative solution to many environmental problems in industrial processes because they provide a versatile, efficient, cost-effective, and "clean reagent" process [15–22]. Da Silva et al. [23,24] recently attempted the electrochemical oxidation of organics through pure water electrolysis with a solid electrolyte. In their reaction system, the liquid acidic solution was replaced by a solid polymer electrolyte; therefore, the problems arising from an aqueous electrolyte were avoided. It was demonstrated that ·OH can be generated by the anode in electrolyte-free water and plays a key role in the oxidation of organics. This finding suggests that gaseous water vapor electrolysis might also proceed on an anode surface to produce ·OH without a conducting medium, which is suitable for indoor VOC elimination under ambient conditions. However, to the best of our knowledge, the application of electrochemical oxidation at a gas-solid interface for gaseous BTX abatement has not been reported to date.

The process of ionic and electron conduction in an all-solid cell is different from that in conventional electrochemical cells using liquid electrolytes. In this case, gas is a non-conductor and the electrochemical reaction only occurs on the gas-electrode-solid polymer electrolyte triple-interface region. Accordingly, it is important for this system to compress the anode and cathode closely against the solid polymer electrolyte, such as in the membrane electrode assembly (MEA) of a fuel cell. Therefore, we designed an MEA for electrochemical oxidation of indoor low-concentration BTX in an all-solid cell. In detail, an antimony-doped SnO_2 catalyst was coated onto the surface of porous Ti foam to act as the anode, and reduced graphene oxide/carbon fiber paper-supported Pt (Pt/rGO/CFP) was employed as the cathode. The ·OH generated from H_2O vapor discharge participates in the VOC oxidation process. The protons produced in the H_2O vapor discharge process at the surface of the anode move inside the Nafion membrane towards the cathode and recombine with O_2 and electrons, resulting in the oxygen reduction reaction (ORR). The electrons originating from the anode pass via the external circuit to the cathode. It was observed that BTX were efficiently and very selectively decomposed into CO_2 by this gas-solid interface electrocatalytic oxidation process at ambient temperature, indicating that this method is promising for indoor air purification applications. We further found that the atmospheric ·OH radicals generated from H_2O vapor discharge were responsible for the gaseous VOC oxidation.

2. Experimental

2.1. Preparation of the anode

A piece of titanium foam (Φ30 mm × 2 mm) was firstly polished with abrasive paper and etched with 20% (w/w) NaOH at 80 °C for 0.5 h and with a 10% oxalic acid solution for 2 h, respectively. The substrate was then washed with doubly distilled water by ultrasonic washing. Sb-SnO_2 was loaded onto the titanium foam plate by a two-step method [25]. An interlayer Sb-SnO_2 coating was fabricated by electrodeposition, and an outer layer coating was applied using a brush coating-pyrolysis process. A mixture of Sn and Sb electrodeposition on the Ti foam plate was carried out at room temperature using a two-electrode system (1 cm separation) with a Ti foam plate serving as the cathode and Pt sheet serving as anode. An ethanediol solution containing 1 M $SnCl_4$, 0.2 M $SbCl_3$ and 0.1 M HNO_3 was used as the electroplating bath, with a current density of 15 mA cm^{-2} for 1 h. After electrodeposition of Sn and Sb, the electrode was heated in an oven at 773 K for 1 h and then cooled in air, and oxides of Sn and Sb formed on the Ti foam substrate. A solution mixture of isopropanol and n-butanol containing 0.5 M $SnCl_4$, 0.02 M $SbCl_3$, 1 M HNO_3 and 0.01 M NaF was brushed on the oxidized Sn and Sb interlayer. After brush-coating, the sample was dried in an oven at 373 K for 5 min, calcined at 773 K for 30 min, and then cooled in air. The brush coating procedure was repeated until the loading amount of the coating on the electrode attained 28.7 mg cm^{-2}, and the sample was referred to as SS-28.7/Ti.

2.2. Preparation of the cathode

The Pt/rGO/CFP electrode was prepared by electrochemically depositing Pt on a GO film, which was chemically reduced in situ on the CFP. The CFP substrate consisted of carbon fibers with diameters of approximately 8–10 μm. Prior to use, the CFP was firstly immersed in a 0.1 wt% Triton X-100 solution for 24 h and then ultrasonically treated in deionized water for 2 h to lower the hydrophobicity. Then, the CFP was heated at 400 °C for 5 h to increase the number of oxygen-containing functional groups on the surface and the level of impregnation in the GO dispersion in the next step. The CFP was immersed in a 2 mg/mL GO suspension to adsorb GO. Subsequently, the GO film-coated CFP was immersed in a 10 mg/mL ascorbic acid solution overnight and then heated at 60 °C for 2 h. After chemical reduction of the GO film (rGO), Pt was electrochemically deposited on the rGO/CFP electrode from an aqueous solution of 10 mM NH_4Cl containing 1 mM $PtCl_4$ (pH = 1) at a constant current of 20 mA for 120 min.

2.3. Physicochemical characterization

The morphology of the electrodes was characterized using scanning electron microscopy (SEM, Merlin, Carl Zeiss, Germany) coupled with

energy dispersive spectroscopy (X-MAX, Oxford Instrument). X-ray powder diffraction patterns (XRD) of the Sb-SnO_2/Ti anodic electrode and Pt/rGO/CFP cathodic electrode were obtained with an X'Pert PRO powder diffractometer (XRD, Rigaku D/max, Rigaku Co.) using Cu Kα radiation scanning from 10° to 90° (in 2θ). The surface composition and chemical state of the samples were examined by X-ray photoelectron spectroscopy (XPS) using a scanning X-ray microprobe (Axis Ultra, Kratos Analytical Ltd.) and Al Kα radiation (1486.7 eV). The C1s peak (284.8 eV) was used to calibrate the binding energy (BE) values. The concentrations of Pt^{4+}, Sn^{4+} and Sb^{3+} in the electrolyte were measured by an 8300 inductively coupled plasma optical emission spectrometer (ICP-OES, PerkinElmer Inc.) to quantify the Pt, Sn and Sb loading amounts on the electrodes.

2.4. Electrochemical oxidation tests for benzene, toluene and xylene

2.4.1. Setup

Fig. 1 illustrates the schematic diagram of the experimental setup for the electrochemical oxidation of VOCs in flow mode. The testing system consisted of a CHI 760E electrochemical workstation (CH Instrument. Co. Ltd., Shanghai China), an all-solid reactor, a 2 L anodic reactant gas reservoir and a detector. The electrochemical reactor was separated into a cathode compartment and an anode compartment by the membrane electrode assembly (Fig. 1, bottom right). Each compartment of the all-solid reactor was fed with gaseous streams. The cathodic feed was a flow of 80% N_2 and 20% O_2. The reactant gases in the anodic compartment contained BTX, O_2 (20%) and N_2 balance with relative humidity varying from 0 to 60%. The anodic reactant was recirculated via a pump from the gas reservoir, flowing through the reactor and the detector with a flow rate of 100 mL/min. The BTX was supplied by cylinder gas (Beijing huayuan gas chemical Co., Ltd.). The contents of BTX were 40 ppm (benzene), 88 ppm (toluene), 45 ppm (o-xylene).

The relative humidity was regulated by adjusting the dry feed gas to bubble through a humidity control unit including a cold-water circulation apparatus (CCA-20, Gongyi Yuhua Instrument Co., Ltd) and a hygrometer (314, Taiwan Center technology Co.), which controlled the temperature of the pure water in the bottle and monitored the humidity of the reactant stream. For the BTX electrochemical oxidation tests, potentiostatic electrolysis was performed with an electrochemical workstation at cell voltages of 1.0, 2.0 and 3.0 V. The protons produced in the H_2O vapor discharge process at the surface of the anode move inside the Nafion membrane towards the cathode and recombine with O_2 and electrons, resulting in the oxygen reduction reaction (ORR). The electrons originating from the anode pass via the external circuit to the cathode. Thus, there is no pH change at the surface of the anodic active centers, avoiding corrosion of the anodic materials.

2.4.2. Membrane electrode assembly

The schematic diagram of the all-solid electrochemical reactor and MEA is given in Fig. S1. A 4.0 × 4.0 cm Nafion membrane was used as the electrode separator and solid polymer electrolyte. The Nafion membrane was pre-treated by immersion in boiling 50% HNO_3 solution for 30 min and then in boiling deionized water for 2 h to provide adequate hydration of the membrane [23,26,27]. SS-28.7/Ti and Pt/rGO/CFP acted as the anode and cathode. The Pt/rGO/CFP cathode was attached on one face of the membrane with a few drops of the Nafion solution (left to dry for 10 min in air). A pressure of 0.6 MPa cm^{-2} was applied to compress the anode and cathode against the solid polymer electrolyte to prevent gaps and membrane cracking.

2.5. Product measurement

2.5.1. Anodic product measurement

The anodic reactants and products were analyzed online using a GC2014C gas chromatograph (Shimadzu, Japan) equipped with a flame ionization detector (FID). An Rtx-Wax strongly polar capillary column was used for the high-sensitivity analysis of BTX (benzene, toluene, xylene), alcohols, aldehydes, acids and phenols. Two packed columns (Porapak-N and MS-13X) were utilized for the analysis of the anodic products, CO_2 and CO. A proton-transfer-reaction mass spectrometry (PTR-MS, QiTOF-008, Ionicons) was used to detect the gaseous

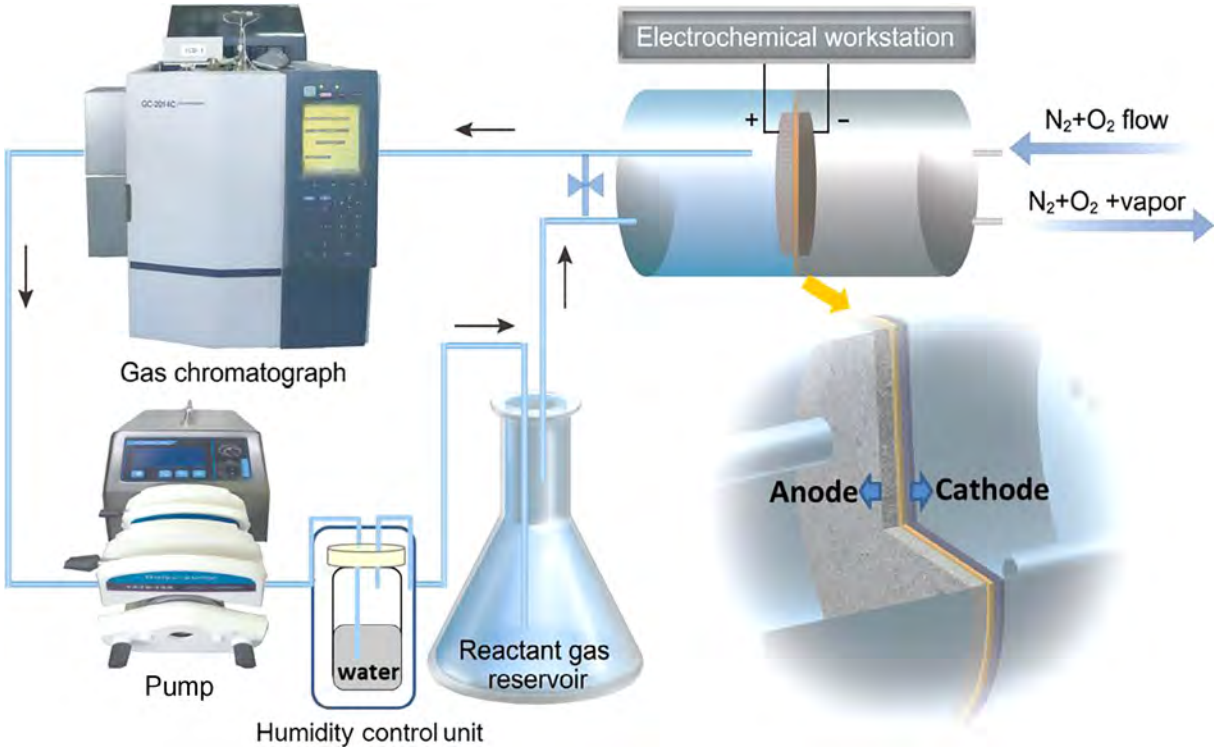

Fig. 1. Schematic diagram of the experimental setup used in the electrochemical oxidation of VOCs under flow conditions.

products in the range of m/e from 40 to 200. An FTIR spectrometer (Nicolet 380) equipped with 2 m gas cell and a DTGS detector was used to collect the infrared spectra in the range of 4000–800 cm^{-1}. The 2.0 L anodic reactant gas circularly flowed over the reactor and the detector. The initial concentration of reactant gas was 40 ppm benzene, 20 vol% O_2, and N_2 balance. A spectrum in a flow of the initial feed gas was firstly collected as the background spectrum.

Since benzene can be electro-oxidized to CO_2 and CO (CO_x), the overall process can be considered to occur as follows:

$$C_6H_6 + 6H_2O \rightarrow 6CO + 18H^+ + 18e^-$$

$$C_6H_6 + 12H_2O \rightarrow 6CO_2 + 30H^+ + 30e^-$$

$$\text{Benzene conversion}(\%) = \frac{C_0 - C}{C_0} \times 100$$

$$\text{CO or } CO_2 \text{ yield}(\%) = \frac{\Delta C_{cox}/6}{C_0} \times 100$$

where c_0 and c are the concentrations of benzene initially and at time t, respectively. Δc_{cox} is the experimental value for the CO or CO_2 yield at time t.

The mineralization current efficiency (MCE) at a given time t for the treated gaseous benzene is then estimated as follows:

$$MCE = \frac{\Delta(TOC)_{exp}}{\Delta(TOC)_{theor}} \times 100\%$$

where $\Delta(TOC)_{exp}$ is the experimental value for TOC removal at time t and $\Delta(TOC)_{theor}$ is the theoretical value of calculated TOC removal, which can be calculated as follows:

$$\Delta(TOC)_{theor} = \frac{\frac{It}{n_e F} \times n_c \times 12 \times 10^3}{V} mg \cdot L^{-1}$$

where I is the current intensity (A), t is electrolysis time (s), F is Faraday constant, 96,485 $C \cdot mol^{-1}$. n_e is the electron transfer number, n_c is the carbon number of the organic compound, M is carbon atomic weight, $M = 12\ g \cdot mol^{-1}$, and V is the volume of the sample solution (L). For benzene conversion to CO_2, n_e and n_c are 30 and 6, respectively. For benzene conversion to CO, n_e and n_c are 18 and 6, respectively.

2.5.2. Cathodic product measurement

As possible products of the cathodic reaction, H_2, H_2O_2 and H_2O were measured. The H_2 concentration was analyzed online by a GC (Agilent 6890-5973N), which was equipped with TCD detectors. H_2O_2 was determined using the 2,9-diamethyl-1,10-phenanthroline (DMPHEN, Aldrich) method ($\lambda = 454$ nm) with copper(II) ions ($CuSO_4 \cdot 5H_2O$, Aldrich) [24].

2.6. Mechanism of electrocatalytic oxidation of BTX

2.6.1. Electrochemical characterization

To observe the oxidation of water and organics on the surface of SS-28.7/Ti in the solid polymer electrolyte cell [23,24,26], cyclic

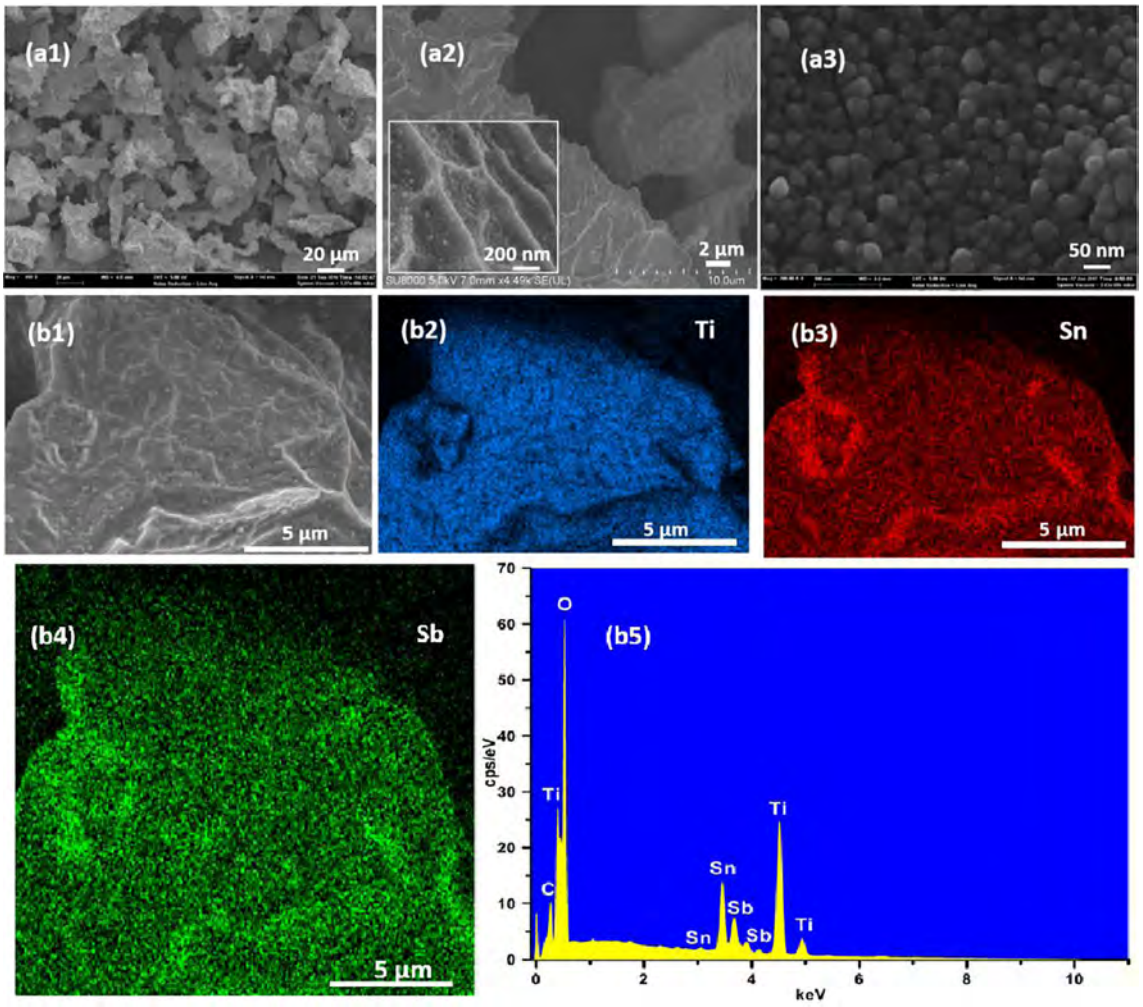

Fig. 2. (a) SEM images and (b) energy dispersive X-ray spectroscopy (EDX) results of the SS-28.7/Ti electrode: (b1-b4) secondary electron image and X-ray dot map of Sn, Sb and Ti, and (b5) elemental analysis.

voltammetry measurements were performed using a two-compartment cell with the MEA serving as the separator. SS-28.7/Ti with a diameter of 2.0 cm served as working electrode, and a KCl-saturated Ag/AgCl and Pt/rGO/CFP separately served as reference and counter electrodes. In the anodic compartment, 20 ppm or 40 ppm benzene were added in ultra-pure water. The experiment was performed at a scan rate of 10 mV s^{-1} from −0.5 to 3.0 V. Experimental data were obtained from the tenth voltammetric cycle. Voltammetric curves were also recorded in a 0.1 M H_2SO_4 solution. Chronoamperometric experiments were carried out to test the electrocatalytic response of water and benzene on the SS-28.7/Ti electrode at constant potentials of 0, 1, 2 and 3.0 V (vs Ag/AgCl, saturated KCl). All the potentials were referred to Ag/AgCl. Ultra-pure water with a resistivity of 18.2 MΩ cm^{-1} at 25 °C was obtained using a Genpure Pro ultrawater purification system (UV-TOC xCAD plus, Thermo scientific).

2.6.2. ROS measurement

·OH radicals generated by water vapor discharge on the surface of the anode were measured by gas expansion and fast gating laser-induced fluorescence techniques. Ambient air at a flow rate of 1.5 L/min entered a low-pressure fluorescence cell through a molecular beam skimmer (Beam Dynamics, USA) with an orifice diameter of 1 mm, and was irradiated by a combination of Nd:YVO_4 and tunable dye lasers at a high repetition rate of 8.5 kHz. The ·OH radical was excited and detected at 308 nm using the A-X(0,0) band. A microchannel plate photomultiplier (MCP) was designed for the ·OH radical measurements. O_3, as an often-generated species in electrocatalytic oxidation processes [28], was also measured in this study using an O_3 detector (Model 49i, Thermo Fisher Scientific, Inc. USA).

The amounts of aqueous-phase ·OH radicals were quantified by colorimetric methods using a 2100 UV − vis absorption spectrophotometer (UNIC, France). The ·OH radicals were estimated at λ = 440 nm using N,N-dimethyl-4-nitrosoaniline (RNO, 1 mM) as a quencher [18,28].

3. Results and discussion

3.1. Characterization of the anodic and cathodic electrodes

Antimony-doped SnO_2 (Sb-SnO_2), which has excellent electrocatalytic performance, is regarded as one of the most effective anode materials for the electrochemical oxidation of organic pollutants in wastewater [23,24,27–36]. Considering that gas-permeable electrodes are necessary for a gas-phase reaction to occur on a membrane electrode assembly, in this study, a porous Ti metal foam was selected as the substrate to fabricate the Sb-SnO_2/Ti anode (referred to as SS-28.7/Ti).

SEM images of the original and etched foam Ti substrate are presented in Fig. S2. The fresh Ti foam has a smooth surface, and the etching procedure in boiling 20% oxalic acid clearly increased the surface roughness of the Ti foam, which is favorable for the deposition of a Sb-SnO_2 layer. The surface morphology of the Sb-SnO_2 coating on the Ti foam is presented in Fig. 2. A compact and homogeneously dispersed Sb-SnO_2 nanoparticle layer with an average particle size of approximately 37.5 nm was fabricated on the Ti foam substrate, as shown in Fig. 2(a1–a3). On the conventional Ti plate substrate, an Sb-SnO_2 coating usually forms a “cracked-mud” surface structure, and the particle size can be up to hundreds of nm (Fig. S2(c)) [31–35]. Here, we successfully prepared a crack-free nanoparticle Sb-SnO_2 coating on the Ti foam substrate, possibly due to the porous structure of the Ti foam. The porous structure is favorable for the diffusion of the precursor solution during fabrication of the compact crack-free nanoparticle film.

X-ray dot-mapping was used for an analysis of the metal distributions. As shown in Fig. 2(b1–b4), the mapping images demonstrated a homogeneous distribution of Sn and Sb in the oxide films on the Ti foam surface. The elemental analysis results (Fig. 2(b5) and Table 1) show that the content of Sb in the Sb-SnO_2 coating film is approximately 5 mol%; therefore, the film coating exhibits the lowest resistivity reported in this material system (1×10^{-3} Ω cm^{-1}), as mentioned in a previous study [29]. Since Ti was detected, the thickness of the Sb-SnO_2 coating was lower than 500 nm, which is the EDX detection depth.

X-ray diffraction patterns of Sb-SnO_2 supported on the Ti foam substrate and Ti plate are shown in Fig. S3. The SS-28.7/Ti electrode only showed sharp peaks related to the Ti support, while no characteristic peaks of Sn and Sb oxides appeared, possibly because the Sb-SnO_2 layer was too thin (lower than 20 μm) to be detected. For comparison, we also measured the XRD pattern of a Ti plate-supported 28.7 mg cm^{-2} Sb-SnO_2 sample. This sample presented strong diffraction peaks for cassiterite SnO_2 (PDF# 41-1445), but no Ti peaks were detected [25,34–36]. Considering that the same preparation method was used, we confirmed that a Sb-SnO_2 layer was formed on the Ti foam substrate, but that its thickness on the Ti foam was much lower than that on the Ti plate. No additional peaks appeared corresponding to the antimony oxides, perhaps due to the low doping level or the incorporation of Sb in the SnO_2 unit cell.

X-ray photoelectron spectroscopy was employed to analyze the chemical states of the elements. Fig. S4 shows the XPS spectra of the Sn 3d and Sb 3d binding energies of the Sb-SnO_2 layer on SS-28.7/Ti. The Sn $3d_{5/2}$ binding energy in the electrode was 487.0 eV, which agrees with the $Sn3d_{5/2}$ binding energy in a SnO_2 crystal or $Sn(OH)_4$ hydroxylated species [28,32]. The two peaks centered at 530.6 and 540.1 eV can be assigned to Sb $3d_{5/2}$ and Sb $3d_{3/2}$ of Sb_2O_5, respectively. The molar ratio of Sn/Sb in the electrodes was 16.6, which is lower than that of the precursor solution (25:1), possibly due to Sb enrichment on the surface of the layer [32].

For the cathodic ORR, most electrocatalysis research has focused on Pt-based catalysts due to their great application potential [37–40]. Graphene, a two-dimensional material consisting of a monolayer of carbon atoms, has high electrical conductivity, mechanical strength and surface area [41–43]. Thus, the combination of Pt and graphene will enhance the electrochemically active surface area and facilitate the high dispersion of Pt, and effectively accelerate the electron transfer, leading to a more rapid kinetics of O_2 reduction [37–43]. Carbon fiber paper (CFP) has low electrical resistivity, minimal electrochemical corrosion and good gas permeability. Therefore, in this study, CFP was used as the substrate material for preparation of the cathode. The Pt-reduced graphene oxide-modified carbon fiber paper (Pt/rGO/CFP) electrode was prepared by electrochemically depositing Pt on the GO film, which was chemically reduced in situ on the CFP. The loading amount of Pt on the Pt/rGO/CFP electrode was determined to be 0.9 mg cm^{-2} by ICP-OES. Fig. S5 shows the SEM images and XRD patterns of the Pt/rGO/CFP electrode.

3.2. Electrocatalytic degradation of VOCs

The gas-solid interface electrocatalytic oxidation of VOCs was performed on the membrane electrode assembly at room temperature. Common and intractable industrial emissions, such as benzene, toluene

Table 1
EDX analyses of the benzene SS-28.7/Ti electrode before and after electrochemical oxidation.

Characteristic X-ray (energy, hν/keV)	Freshly prepared electrode		Post-electrolysis electrode	
	At %	Error %	At %	Error %
Ti (4.508)	30.36	0.13	29.12	0.06
Sn (3.442)	5.89	0.09	5.65	0.11
Sb (3.603)	0.33	0.03	0.32	0.12
O (0.277)	58.17	0.1	55.8	0.08
C (0.525)	5.23	0.03	5.02	0.03

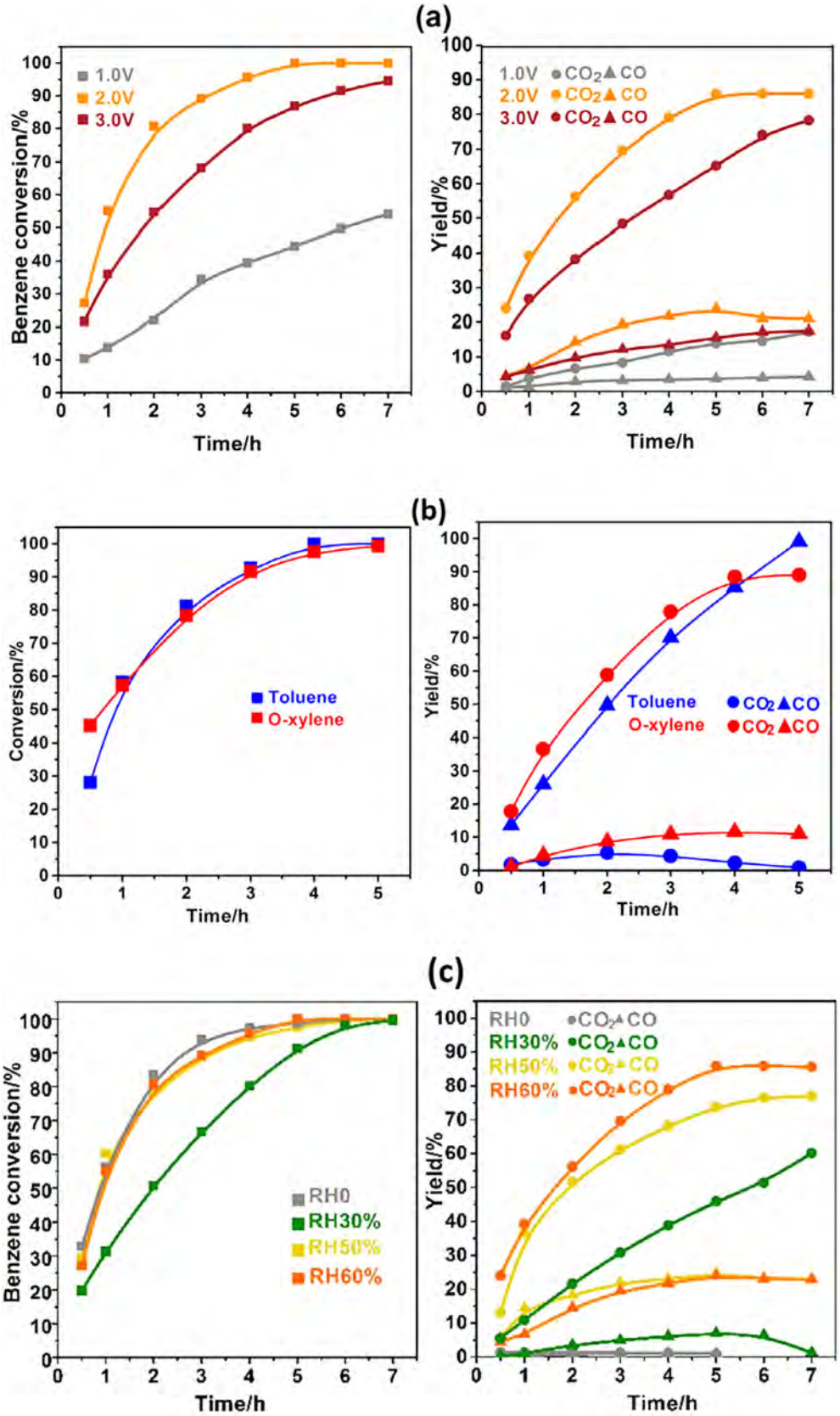

Fig. 3. (a) Effects of the applied cell voltage on the activity of the SS-28.7/Ti electrodes for the conversion of 40 ppm benzene to CO_x at relative humidity 60% (b) the conversion of 88 ppm toluene and 45 ppm o-xylene at an applied cell voltage of 2.0 V at relative humidity 60%. (c) The effect of the relative humidity of the reactant gas on the activity of the SS-28.7/Ti electrodes for conversion of benzene to CO_x.

and o-xylene (BTX), were selected as the model VOCs. The effect of the cell voltage on benzene removal was investigated. As shown in Fig. 3(a), benzene conversion was poor at the 1.0 V cell voltage, and the conversion of benzene to CO_x was below 20% within 5 h. When the cell voltage was raised to 2.0 V, 100% benzene conversion to CO_2 (85%) and CO (15%) was achieved in the same time interval. Further, benzene conversion and CO_2 selectivity decreased to some degree when the voltage was increased to 3.0 V. The gas composition of the products of the electrochemical oxidation of benzene was also confirmed by means of a Fourier transform infrared spectrometer (FTIR) equipped with a gas cell. Toluene and o-xylene were also completely electro-oxidized to CO_x within 4 h, and the CO_2 yield reached 90% and 99%, respectively (Fig. 3(b)). These results suggest that the gas-solid interface electrocatalytic oxidation system effectively converted the VOCs to CO_x at room temperature.

The effect of humidity on the conversion of benzene to CO_x was also investigated. As shown in Fig. 3c, when no water vapor was present in the reactant gas, 100% of the benzene was removed after 5 h, but no CO_x was produced, indicating that only the adsorption of benzene occurred on the anode and no direct electrolysis of benzene occurred without water vapor. With increasing humidity in the reactant gas stream, the benzene conversion and CO_x yield were both promoted. It can be inferred that the direct electrochemical oxidation of benzene cannot occur on the electrode at the applied cell voltage of 2.0 V, and the gas-solid electrochemical oxidation of benzene mainly resulted from indirect electrolysis with ROS generated from water vapor discharge.

From Fig. 3c, the conversion of benzene at RH = 30% was lower than that at RH = 0. This is probably due to competitive adsorption between water vapor and benzene on the active sites of the anode. The adsorbed water vapor occupied the active sites for benzene adsorption, resulting in the conversion of benzene being decreased. Since the ·OH radicals were generated from the adsorbed water vapor discharge at RH = 30%, the oxidation of benzene to CO_x occurred. However, the yield of ·OH radicals was not high enough to totally convert the adsorbed benzene. When the RH reached 60%, the yield of ·OH was enhanced, then increasing the conversion of the adsorbed benzene to CO_x. Therefore, the amount of ·OH is key to the mineralization of benzene.

Three successive cycles of electro-oxidation experiments with initial concentration 40 ppm gaseous benzene were further carried out. As shown in Fig. S6, the efficiency for benzene conversion remained almost constant from the first to the third run, and the CO_2 yield showed a moderate reduction from 80% to 70%. The reduction of selectivity for CO_2 may result from carbon accumulation on the surface of the electrode. As mentioned in a recently reported study [44], the structural

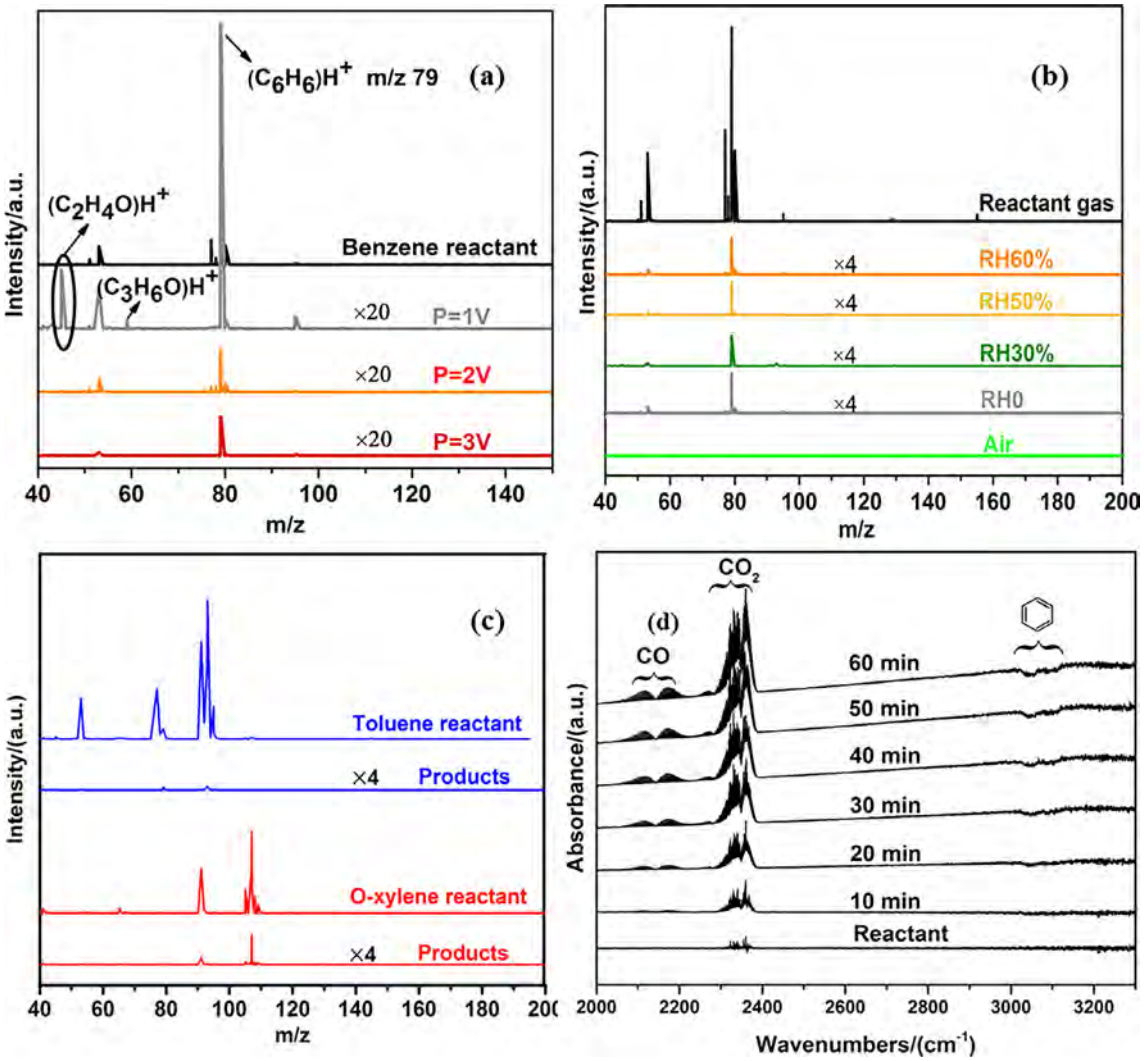

Fig. 4. PTR-Mass signal for (a) reactant gas and gaseous products of benzene after electrolysis with different applied cell voltages at 60% humidity, (b) benzene reactant gas and gaseous products after 7 hr electrolysis with 2.0 V cell voltage at humidity of 0, 30%, 50% and 60%, (c) toluene and o-xylene reactants and their products after electrolysis with 2.0 V cell voltage at 60% humidity. (d) Fourier Transform infrared spectroscopy of reactant and products during electrolysis of benzene with 2.0 V cell voltage at 60% humidity.

characteristics had a great influence on the durability of the studied materials. TiO_2 nanoparticles underwent rapid deactivation during repeated photocatalytic degradation cycles of VOCs. TiO_2 nanotubes with open channels were markedly more resistant to deactivation than TiO_2 nanoparticles. The open, straight-channel structure of TiO_2 nanotubes facilitates the mass transfer of O_2 onto the active sites, accelerates the photocatalytic degradation of intermediates and hinders the accumulation of carbonaceous residues. Accordingly, in future work, we will try to synthesize an electrode using a nanotube material to avoid carbon accumulation and promote the resistance to deactivation.

The energy consumption of BTX mineralization was calculated, and the results were 0.12 kWh/g toluene, 0.27 kWh/g o-xylene, and 0.44 kWh/g benzene, at 50% removal of BTX. The mineralization current efficiency (MCE) value for the electro-oxidation of gaseous 40 ppm benzene was about 5% at first hour electrolysis and decreased to 3% at 5-hour electrolysis, shown in Fig. S7. The present MCE values were lower than that in electrochemical degradation of pollutant in water treatment [50], which is probably due to the low initial concentration of BTX resulting in the low utilization efficiency of ROS. In future work, to promote the adsorption and enrichment of VOCs on the anode, some materials with huge specific surface areas, such as carbon materials, can be used as electrode substrates.

3.3. Details of products

Proton-transfer-reaction time-of-flight mass spectrometry (PTR-ToF-MS) is considered as one of the most promising direct injection mass spectrometry techniques for simultaneously identifying gaseous organics over a wide mass range with high sensitivity and time resolution [45–47]. Therefore, we further analyzed the gaseous products of BTX oxidation using PTR-ToF-MS. As shown in Fig. 4a, after the 7-hr electrocatalytic oxidation of benzene in 60% humidity conditions, trace amounts of C_2H_4O and C_3H_6O were detected when the potential was 1.0 V, indicating that incomplete oxidation of benzene occurred at low applied cell voltage. In contrast, when a cell voltage higher than 2.0 V was applied, no organic byproducts were detected in the anodic reservoir beyond the components of the feed gas at different levels of humidity (in Fig. 4b and c) after 7 hr electrolysis. When the relative humidity of the reactant gas was 0, CO_2, CO and organic products were not detected, as shown in Fig. 3c and 4b; these results confirm that only the adsorption of benzene occurred on the anode without water vapor.

Additionally, the gaseous products of benzene electrochemical oxidation were also characterized by a Fourier Transform Infrared Spectrometer (FTIR). A spectrum in a flow of the initial feed gas with 40 ppm gaseous benzene was firstly collected as the background spectrum, signed as “Reactant” shown in Fig. 4d. In the electro-oxidation of benzene, when benzene was consumed, a negative peak at 3000–3200 cm^{-1} related to benzene appeared. With the increasing consumption of benzene, this wide peak was getting more negative together with increases in the peak intensities of CO_x (CO: ~2100 cm^{-1}; CO_2: ~2350 cm^{-1}), and no other species were observed in the range from 2000 cm^{-1} to 3000 cm^{-1} during the benzene oxidation process. These results indicate that the benzene was oxidized to CO_x in the electrolysis.

During electrolysis, the aromatic ring opens and possibly decomposes into organic intermediates, such as benzoquinone and carboxylic acids [18,25,48–50]. These compounds are difficult to degrade and therefore will form a polymer layer on the anode, resulting in electrode fouling. To test the formation of intermediates on the anode surface, EDX, XPS and SEM were conducted on the SS-28.7/Ti electrode before and after the electrochemical oxidation of benzene. Elemental information on the electrode surface was obtained by EDX. The concentrations of the elements were calculated by integrating the peak areas. As shown in Table 1, the concentrations of Sn, Sb and C on the electrodes after the reaction remained nearly the same as those on the freshly prepared Sb-SnO_2/Ti, indicating the high stability of the electrode and lack of intermediates/byproducts on the electrode surface. These results were also confirmed by XPS, which showed no noticeable change in the C 1s region between the freshly prepared and used SS-28.7/Ti electrodes (in Fig. S8). The detected carbon was attributed to organic solvent residuals used in the electrode preparation process. SEM images were also collected to identify the electropolymerized film

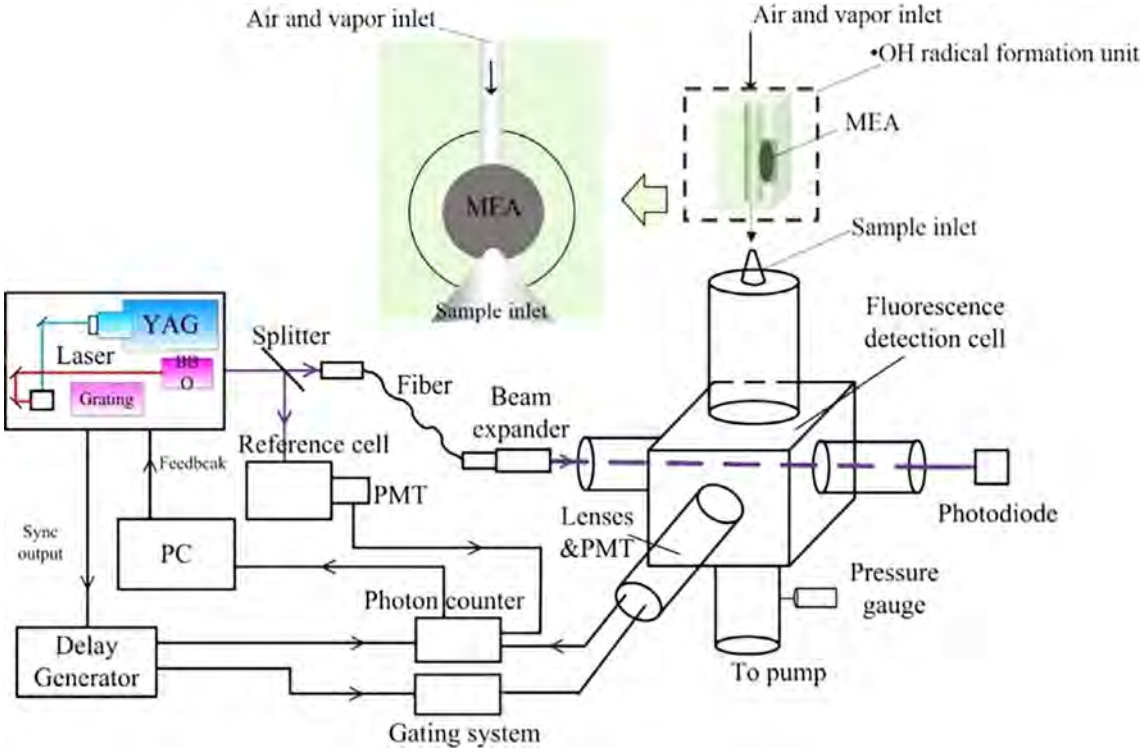

Fig. 5. Scheme diagram of·OH radical detection system with gas expansion and fast gating laser-induced fluorescence.

on the electrode surface [48]. The images show that no solid matter was present on the surface of the nanoparticles after the electrolysis of benzene (Fig. S8). These results show that no gaseous organic by-products or solid matters were present during the electrolysis of BTX with applied cell voltage exceeding 2.0 V. Hence, the electro-oxidation of gaseous organic pollutants by the gas-solid cell is suitable for indoor gaseous VOC elimination under ambient conditions.

3.4. Mechanism of electrochemical oxidation of VOCs in all-solid cell

3.4.1. ROS measurements

In the electrochemical degradation tests of BTX, when no water vapor was present in the influent, little or no BTX was converted into CO_x, as shown in Fig. 3c. In addition, considering the high oxidation potentials of BTX ($E^0_{benzene}$ = 2.86 V_{NHE}, $E^0_{toluene}$ = 2.49 V_{NHE}, E^0_{xylene} = 2.4 V_{NHE} [51]), these intractable VOCs could not be directly oxidized at the low cell voltage used. It can be concluded that ROS generated from water vapor discharge were key to the mineralization of BTX at the 2.0 cell voltage.

Laser-induced fluorescence (LIF) is a reliable and efficient tool for the direct detection of atmospheric ·OH [52], with a detection limit of approximately 10^5 molecules/cm^3. To confirm that the ROS generated from water vapor discharge in the all-solid cell were ·OH radicals, we employed an LIF instrument to directly measure the atmospheric ·OH radicals dissociated from the surface of the anode, and a schematic of the instrument is shown in Fig. 5. We designed and set up an all-solid electrochemical reactor connected to the LIF instrument (·OH radical formation unit, shown in Fig. 5), where the surface of the anodic electrode was in close proximity to the sample inlet, and the diameter of the gas flow was 3 mm. The air/water vapor stream was pumped to the sample inlet after sweeping past the electrode surface; therefore, the gaseous ·OH radicals generated from the electrode surface were instantaneously drawn into the chamber and then detected by LIF. The diffusion time of the generated ·OH radicals from the anode surface to the detector was less than 13.5 ms, which is far less than the ~1 s lifetime of atmospheric ·OH [53]. In Fig. 6, the background ·OH signal was recorded with irradiation at the laser light off-resonance, when air with 40% relative humidity passed through the reactor. When a 2.0 V cell voltage was applied on the MEA, the variation in the concentration of ·OH radical was measured. The concentration of gaseous ·OH radicals diffusing from the electrode reached 2.5×10^6 molecules/cm^3. According to the current intensity of the water vapor discharge (tens of mA) and the subsequent UV–vis absorption results for ·OH radicals (shown in Fig. S9), the ·OH radical yield was approximately 10^{18} molecules/cm^3. The lower concentration of ·OH radicals detected by LIF possibly resulted from dilution of the generated ·OH radicals by the air flow, and the quenching of hydroxyl radicals due to turbulence, etc. After electrolysis for 1 h, the power was switched off, and the ·OH signal gradually returned to the background level. The above findings confirm the generation of ·OH radicals from water vapor discharge on the surface of the SS-28.7/Ti anode at a 2.0 V applied potential. These results indicate that LIF can be considered a feasible method to detect ·OH radicals at a gas-solid interface because of its adequately high sensitivity and low detection limit.

Additionally, traditional colorimetric methods [19,28,30] were used to quantify the ·OH radicals generated from water molecule discharge without the addition of a conducting reaction medium at the SS-28.7/Ti anode surface. N,N-dimethyl-4-nitrosoaniline (RNO) was used as a quencher to detect and quantify ·OH radicals using a UV–vis absorption spectrophotometer, and the results are shown in Fig. S9. The

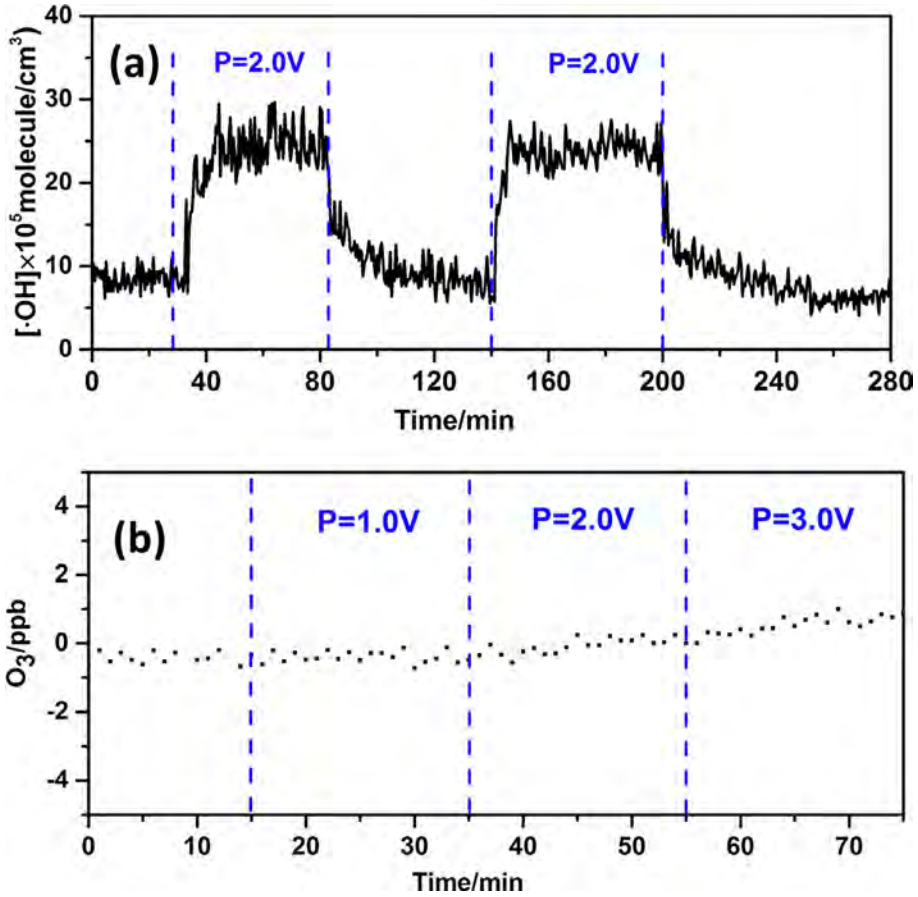

Fig. 6. (a) Electrocatalytic generation of ·OH radicals measured by laser-induced fluorescence. The excitation line of the ·OH radicals was at 308 nm. (b) Time profiled anodic production of O_3 at P_{cell} = 1.0–3.0 V.

yield of ·OH radicals reached 35 μmol within 30 min, indicating the high efficiency of the ·OH radical yield compared with previously reported values for the electrocatalytic generation and photogeneration of ·OH [28,30]. The membrane electrode assembly promoted H^+ transmission from the anode to the cathode and therefore increased the reaction rate. Moreover, in the all-solid cell, collisions of ·OH with ions were also avoided by the lack of a conducting reaction medium. Therefore, ·OH radical generation by this method is highly efficient, and is responsible for the high yield of CO_2 in the BTX electrooxidation process. O_3 is a ROS that usually appears in electrochemical water treatment, therefore the O_3 concentration was also measured during the gas-solid interface electrocatalytic oxidation. As shown in Fig. 6(b), when the applied cell voltage was lower than 2.0 V, no O_3 was generated; when the cell voltage was raised to 3.0 V, the O_3 concentration was lower than 1 ppb. Therefore, the contribution to benzene conversion by O_3 is negligible. Literature reports suggest that electrode materials with high overpotential for the OER, in fluoro-compound aqueous electrolytes and at low temperature tend to exhibit high efficiency ozone production [54]. Accordingly, no O_3 was detected in our studied system, probably due to the lack of addition of a supporting electrolyte. Considering the almost complete lack of byproduct formation, the gas-phase electrochemical mineralization of VOCs is superior to other current air pollution treatment technologies, such as photo-assisted technology, plasma and aqueous electro-oxidation technology.

The cathodic products were measured, including H_2, H_2O_2 and H_2O. Except for a small amount of H_2 and H_2O_2 produced at the applied cell voltage of 1.0 V (show in Fig. S10), only water was detected in the cathodic compartment at the cell voltages of 2.0 and 3.0 V, indicating that the oxygen is mainly converted to H_2O on Pt/rGO/CFP. The environment-friendly cathodic products show that the system is suitable for application in indoor air purification.

3.4.2. Electrochemical characterization

To observe the oxidation of water and benzene on the surface of SS-28.7/Ti in the solid polymer electrolyte cell, cyclic voltammetry measurements were performed using a two-compartment cell with an MEA at 25 °C with scanning rates of 10 mV/s in the potential window of −0.5 to 3.0 V. All the potentials are in reference to Ag/AgCl, saturated KCl. As shown in Fig. 7(a), pure water shows a similar response on the SS-28.7/Ti electrode to that obtained on fine stainless steel mesh-supported Sb-SnO_2 electrodes using the same electrolyte [23]. The oxygen evolution reaction (OER) current appeared at a high potential of 2.0 V (E^0 = 1.23 V_{NHE}). The high oxygen evolution overpotential is helpful for the electrode's accumulation of ·OH and beneficial to the "electrochemical incineration" of organic pollutions [18,31,33,48,49]. After the addition of benzene, there is an obvious increase in the current in the OER region (> 2.0 V), which is due to the appearance of benzene oxidation [31,48,50]. The increase of current induced by the addition of benzene was confirmed in 0.1 M H_2SO_4, as shown in Fig. 7(b). As expected, the CV current density obtained in H_2SO_4 solution was higher compared to that in pure water. The current increase brought about by the injection of benzene in the pure water system at OER region is similar to that in 0.1 M H_2SO_4, confirming that benzene oxidation occurred in the OER region with the solid polymer electrolyte.

Chronoamperometric experiments were performed next to study the benzene response in the high potential area. As shown in Fig. 7(c), anodic currents occurred when the potential was stepped to 1.0 V in pure water without benzene. When the stepped potential was raised to 2.0 V, the current increased due to the water discharge. Then the current greatly increased when the potential was 3.0 V. After the addition of benzene, there was no difference in oxidative current on SS-28.7/Ti electrode at 1.0 V. A slight increase in the current intensity was observed at 2.0 V, and a great promotion of current occurred at 3.0 V. Since the oxidation potential of benzene is E^0 = 2.86 V_{NHE} [51], benzene is difficult to be oxidized directly at 2.0 V. Therefore, almost no current increase occurred with the injection of benzene (Fig. 7) and the

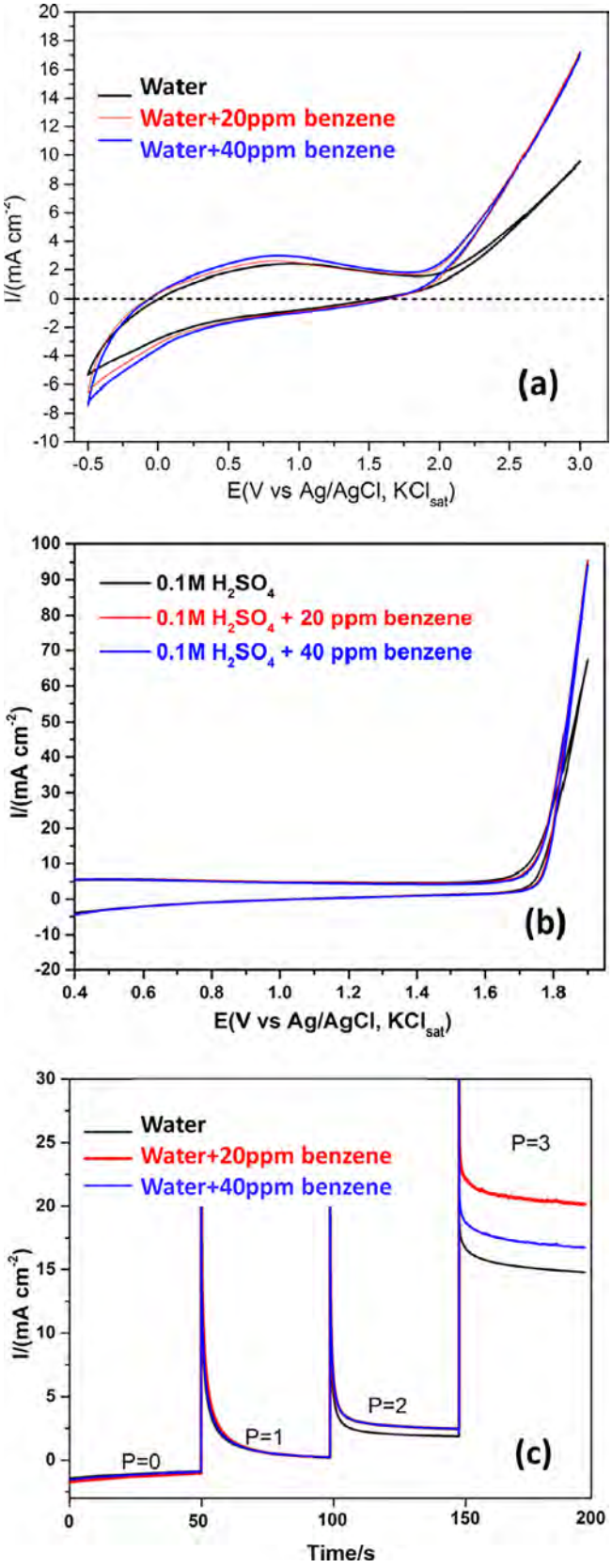

Fig. 7. Cyclic voltammetric curves obtained for SS-28.7/Ti (a) in pure water with and without benzene at a scanning rate of 10 mV s^{-1}, (b) in 0.1 M H_2SO_4 with and without benzene at a scanning rate of 10 mV s^{-1}. (c) Chronoamperometric response of SS-28.7/Ti in pure water with and without benzene.

conversion of benzene to CO_x was also very low (< 10%) with the applied potential of 1.0 V (Fig. 3a). A notable current increase was observed when the applied potential was 2.0 V, which was independent of the benzene concentration, indicating that the ·OH produced on the electrode surface mediated the electrochemical oxidation of benzene [48] and that the benzene oxidation should mainly follow a ·OH-initiated mechanism. When the potential was raised to 3.0 V (in Fig. 7c), the anodic current in pure water sharply increased due to the intensified water discharge. With addition of 20 ppm benzene solution, the anodic current density further increased, while increasing benzene to 40 ppm resulted in a current decrease, but the current was still higher than that in the pure water condition. At the potential of 3.0 V, the direct oxidation process of benzene appeared, therefore both indirect oxidation by electro-generated ·OH and direct electrooxidation were involved in the complex oxidation of benzene.

At the applied cell voltage of 2.0 V, benzene adsorption occurred but no CO_x or organic products were detected in the absence of water vapor (in Fig. 3c), and the current increase was independent of the benzene concentration in water (in Fig. 7c). These findings indicate that indirect oxidation by ROS predominated in the oxidation of benzene. The results of ROS measurement show that the water vapor discharge on the Sb-SnO_2/Ti electrode mainly produced ·OH in the all-solid cell. ·OH reacts with aromatic rings through hydrogen abstraction from the rings [52,55–56]. The powerful oxidant ·OH reacts faster with aromatics compared with other strong oxidants, due to the rapid reaction of ·OH with H of aromatic rings. [52,56] Then, the produced phenol radicals (·Ar-OH) react with O_2 to convert to CO_2. Compared with the aromatics, the oxidation of ·Ar-OH by O_2 has a relatively low activation energy barrier [52,56]. It was deduced that the reaction rate of the oxidation of aromatics by ·OH was higher than that of the direct oxidation of aromatics with oxygen.

When the applied cell voltage was raised to 3.0 V, the direct oxidation of benzene occurred, as shown in Fig. 7c. In the direct oxidation process, the produced Ar^+ favored the formation of a polymeric film on the anode surface, resulting in electrode fouling [51]. Moreover, because the adsorption of aromatics is facilitated by high applied potentials, the higher amount of surface-sorbed species under high concentrations of aromatics occupied more active sites where water discharge could occur [18,48,57,58], resulting in a current decrease in the experiment with 40 ppm benzene. Although the increase in potential can raise the yield of ·OH, the further oxidation of the polymeric intermediates was difficult, and the reaction rate of the mineralization of aromatics to CO_2 dropped off [48,57]. As a result, the hydroxyl radical-mediated oxidation of benzene to CO_x at the potential of 2.0 V showed higher efficiency than that at 3.0 V in electrochemical oxidation of benzene tests, as shown in Fig. 3a.

4. Conclusions

A membrane electrode assembly (MEA) in an all-solid cell was used for electrochemical mineralization of indoor low-concentration gaseous BTX at ambient temperature. At the optimal cell voltage of 2.0 V, BTX were mainly converted to CO_2 (> 85%) at a relative humidity of 60% without the formation of any organic byproducts. The electrochemical behavior of benzene oxidation on the electrode revealed that indirect oxidation via ·OH radicals was responsible for the mineralization of benzene when the potential was at the onset of OER (2.0 V). The present study demonstrates electrochemical oxidation of gaseous BTX in an all-solid cell is a promising method for application in indoor air purification.

Acknowledgments

This work was financially supported by the National Key R&D Program of China (2017YFC0211802, 2017YFC0209401, 2016YFC0207104), and the National Natural Science Foundation of China (51678560, 21577159).

Conflicts of interest

There are no conflicts of interest in this work.

Appendix A. Supplementary data

Supplementary data associated with this article can be found, in the online version, at https://doi.org/10.1016/j.cej.2018.07.208.

References

[1] H. Guo, N.H. Kwok, H.R. Cheng, S.C. Lee, W.T. Hung, Y.S. Li, Formaldehyde and volatile organic compounds in Hong Kong homes: concentrations and impact factors, Indoor Air 19 (2009) 206–217.
[2] P. Wolkoff, Volatile organic compounds—Sources, measurements, emissions, and the impact on indoor air quality, Indoor Air 5 (1995) 1–73.
[3] A. Hodgson, D. Beal, J. McIlvaine, Sources of formaldehyde, other aldehydes and terpenes in a new manufactured house, Indoor Air 12 (2002) 235–242.
[4] W. Jedrychowski, F. Perera, D. Mrozek-Budzyn, E. Mroz, E. Flak, J.D. Spengler, S. Edwards, R. Jacek, I. Kaim, Z. Skolicki, Gender differences in fetal growth of newborns exposed prenatally to airborne fine particulate matter, Environ. Res. 109 (2009) 447–456.
[5] A.P. Jones, Indoor air quality and health, Atmos. Environ. 33 (1999) 4535–4564.
[6] C.J. Weschler, Changes in indoor pollutants since the 1950s, Atmos. Environ. 43 (1) (2009) 153–169.
[7] World Health Organization (WHO), Air Quality Guidelines for Europe, World Health Organization, Geneva, Switzerland, 2000.
[8] Z.X. Zhang, Z. Jiang, W.F. Shangguan, Low-temperature catalysis for VOCs removal in technology and application: a state-of-the-art review, Catal. Today 264 (2016) 270–278.
[9] A.B. Darlington, J.F. Dat, M.A. Dixon, The biofiltration of indoor air: air flux and temperature influences the removal of toluene, ethylbenzene, and xylene, Environ. Sci. Technol. 35 (2001) 240–246.
[10] Y.T. Meng, H.C. Genuino, C.H. Kuo, H. Huang, S.Y. Chen, L.C. Zhang, A. Rossi, S.L. Suib, One-step hydrothermal synthesis of manganese-containing MFI-type zeolite, Mn-ZSM-5, characterization, and catalytic oxidation of hydrocarbons, J. Am. Chem. Soc. 135 (2013) 8594–8605.
[11] A. Luengas, A. Barona, C. Hort, G. Gallastegui, V. Platel, A. Elias, A review of indoor air treatment technologies, Rev. Environ. Sci. Biotechnol. 14 (2015) 499–522.
[12] H.X. Dai, Environmental catalysis: a solution for the removal of atmospheric pollutants, Sci. Bull. 60 (2015) 1708–1710.
[13] J. Georgieva, E. Valova, S. Armyanov, N. Philippidis, I. Poulios, S. Sotiropoulos, Bi-component semiconductor oxide photoanodes for the photoelectrocatalytic oxidation of organic solutes and vapors: A short review with emphasis to Ti_O2-W_O3 photoanodes, J. Hazard. Mater. 211–212 (2012) 30–46.
[14] T. Stoll, G. Zafeiropoulos, I. Dogan, H. Genuit, R. Lavrijsen, B. Koopmans, M.N. Tsampas, Visible-light-promoted gas-phase water splitting using porous WO_3/$BiVO_4$ photoanodes, Electrochem. Commun. 82 (2017) 47–51.
[15] K. Rajeshwar, Electrochemistry and the environment, J. Appl. Electrochem. 24 (1994) 1077–1091.
[16] S. Ma, M. Sadakiyo, M. Heima, R. Luo, R.T. Haasch, J.I. Gold, M. Yamauchi, P.J.A. Kenis, Electroreduction of carbon dioxide to hydrocarbons using bimetallic Cu-Pd catalysts with different mixing patterns, J. Am. Chem. Soc. 139 (2017) 47–50.
[17] C.G. Vayenas, C.G. Koutsodontis, Non-Faradaic electrochemical activation of catalysis, J. Chem. Phys. 128 (2008) 182506.
[18] M. Panizza, G. Cerisola, Direct and mediated anodic oxidation of organic pollutants, Chem. Rev. 109 (2009) 6541–6569.
[19] C. Comninellis, Electrocatalysis in the electrochemical conversion/combustion of organic pollutants for waste water treatment, Electrochim. Acta 39 (1994) 1857–1862.
[20] V.S. Antonin, M.C. Santos, S. Garcia-Segura, E. Brillas, Electrochemical incineration of the antibiotic ciprofloxacin in sulfate medium and synthetic urine matrix, Water Res. 83 (2015) 31–41.
[21] H. Zhao, L. Qian, X. Guan, D. Wu, G. Zhao, Continuous bulk FeCuC aerogel with ultra-dispersed metal nanoparticles: an efficient 3D heterogeneous electro-fenton cathode over a wide range of pH 3–9, Environ. Sci. Technol. 50 (2016) 5225–5233.
[22] H. Zhao, L. Qian, Y. Chen, Q. Wang, G. Zhao, Selective catalytic two-electron O_2 reduction for onsite efficient oxidation reaction in heterogeneous electro-Fenton process, Chem. Eng. J. 332 (2018) 486–498.
[23] I.C. Goncalves, W.T.P. dos Santos, D.V. Franco, L.M. Da Silva, Fabrication and characterization of oxide fine-mesh electrodes composed of Sb-SnO_2 and study of oxygen evolution from the electrolysis of electrolyte-free water in a solid polymer electrolyte filter-press cell: possibilities for the combustion of organic pollutants, Electrochim. Acta 121 (2014) 1–14.
[24] L.M. Da Silva, I.C. Goncalves, J.J.S. Teles, D.V. Franco, Application of oxide fine-mesh electrodes composed of Sb-SnO_2 for the electrochemical oxidation of Cibacron Marine FG using an SPE filter-press reactor, Electrochim. Acta 146 (2014) 714–732.
[25] D. Shao, X.L. Li, H. Xu, W. Yan, An improved stable Ti/Sb–SnO_2 electrode with high performance in electrochemical oxidation processes, RSC Adv. 4 (2014)

21230–21237.
[26] F.R. Costa, L.M. Da Silva, Fabrication and characterization of a porous gas evolving anode constituted of lead dioxide microfibers electroformed on a carbon cloth substrate, Electrochim. Acta 70 (2012) 365–374.
[27] O. Simond, C. Comninellis, Anodic oxidation of organics on Ti/IrO_2 anodes using Nafion® as electrolyte, Electrochim. Acta 42 (1997) 2013–2018.
[28] S.Y. Yang, W.Y. Choi, H.W. Park, TiO_2 nanotube array photoelectrocatalyst and Ni-Sb-SnO_2 electrocatalyst bifacial electrodes: a new type of bifunctional hybrid platform for water treatment, ACS Appl. Mater. Interfaces 7 (2015) 1907–1914.
[29] R. Kotz, S. Stucki, B. Carcer, Electrochemical waste water treatment using high overvoltage anodes. Part I: physical and electrochemical properties of SnO_2 anodes, J. Appl. Electrochem. 21 (1991) 14–20.
[30] S.Y. Yang, D. Kim, H. Park, Shift of the reactive species in the Sb-SnO_2-electrocatalyzed inactivation of *E. coli* and degradation of phenol: effects of nickel doping and electrolytes, Environ. Sci. Technol. 48 (2014) 2877–2884.
[31] L. Ciriaco, D. Santos, M.J. Pacheco, Anodic oxidation of organic pollutants on a Ti/SnO_2-Sb_2O_4 anode, J. Appl. Electrochem. 41 (2011) 577–587.
[32] F. Montilla, E. Morallon, A. De Battisti, S. Barison, S. Daolio, J.L. Vazquez, Preparation and characterization of antimony-doped tin dioxide electrodes. 3. XPS and SIMS characterization, J. Phys. Chem. B 108 (2004) 15976–15981.
[33] C. Pulgarin, N. Adler, P. Peringer, C. Comninellis, Electrochemical detoxification of a 1,4-benzoquinone solution in wastewater treatment, Water Res. 28 (1994) 887–893.
[34] J.F. Liu, Y.J. Feng, Investigation on the electrocatalytic characteristics of SnO_2 electrodes with nanocoating prepared by electrodeposition method, Sci. China Ser. E-Tech. Sci. 52 (2009) 1799–1803.
[35] R. Berenguer, J.M. Sieben, C. Quijada, E. Morallon, Pt- and Ru-doped SnO_2-Sb anodes with high stability in alkaline medium, ACS Appl. Mater. Interfaces 6 (2014) 22778–22789.
[36] X.M. Chen, G.H. Chen, P.L. Yue, Stable $Ti/IrOx-Sb_2O_5-SnO_2$ anode for O_2 evolution with low Ir content, J. Phys. Chem. B. 105 (2001) 4623–4628.
[37] D. Kim, M.S. Ahmed, S. Jeon, Different length linkages of graphene modified with metal nanoparticles for oxygen reduction in acidic media, J. Mater. Chem. 22 (2012) 16353–16360.
[38] Y.M. Li, L.H. Tang, J.H. Li, Preparation and electrochemical performance for methanol oxidation of Pt/graphene nanocomposites, Electrochem. Commun. 11 (2009) 846–849.
[39] S. Guo, D. Wen, Y. Zhai, S. Dong, E. Wang, Platinum nanoparticle ensemble-on-graphene hybrid nanosheet: one-pot, rapid synthesis, and used as new electrode material for electrochemical sensing, ACS Nano 4 (2010) 3959–3968.
[40] Y.G. Kim, Z.A. Akbar, D.Y. Kim, S.M. Jo, S.Y. Jang, Aqueous dispersible graphene/Pt nanohybrids by green chemistry: application as cathodes for dye-sensitized solar cells, ACS Appl. Mater. Interfaces 5 (2013) 2053–2061.
[41] L.H. Tang, Y. Wang, Y.M. Li, H.B. Feng, J. Liu, J.H. Li, Preparation, structure, and electrochemical properties of reduced graphene sheet films, Adv. Funct. Mater. 19 (2009) 2782–2789.
[42] M. Segal, Selling graphene by the ton, Nat. Nanotechnol. 4 (2009) 612–614.
[43] C.C. Huang, C. Li, G.Q. Shi, Graphene based catalysts, Energ. Environ. Sci. 5 (2012) 8848–8868.
[44] S. Weon, W. Choi, TiO_2 nanotubes with open channels as deactivation-resistant photocatalyst for the degradation of volatile organic compounds, Environ. Sci. Technol. 50 (2016) 2556–2563.
[45] D. Papurello, C. Soukoulis, E. Schuhfried, L. Cappellin, F. Gasperi, S. Silvestri, M. Santarelli, F. Biasioli, Monitoring of volatile compound emissions during dry anaerobic digestion of the organic fraction of municipal solid waste by proton-transfer-reaction time-of-flight mass spectrometry, Bioresour. Technol. 126 (2012) 254–265.
[46] J. de Gouw, C. Warneke, R. Holzinger, T. Klupfel, J. Williams, Inter-comparison between airborne measurements of methanol, acetonitrile and acetone using two differently configured PTR-MS instruments, Int. J. Mass Spectrom. 239 (2004) 129–137.
[47] C. Giorio, S.J. Campbell, M. Bruschi, F. Tampieri, A. Barbon, A. Toffoletti, A. Tapparo, C. Paijens, A.J. Wedlake, P. Grice, D.J. Howe, M. Kalberer, Online quantification of criegee intermediates of α-pineneozonolysis by stabilization with spin traps and proton-transfer reaction mass spectrometry detection, J. Am. Chem. Soc. 139 (2017) 3999–4008.
[48] J.F. Zhi, H.B. Wang, T. Nakashima, T.N. Rao, A. Fujishima, Electrochemical incineration of organic pollutants on boron-doped diamond electrode. Evidence for direct electrochemical oxidation pathway, J. Phys. Chem. B 107 (2003) 13389–13395.
[49] X. Li, Y. Cui, Y. Feng, Z. Xie, J. Gu, Reaction pathways and mechanisms of the electrochemical degradation of phenol on different electrodes, Water Res. 39 (2005) 1972–1981.
[50] G. Zhao, X. Cui, M. Liu, P. Li, Y. Zhang, T. Cao, H. Li, Y. Lei, L. Liu, D. Li, Electrochemical degradation of refractory pollutant using a novel microstructured TiO_2 nanotubes/Sb-doped SnO_2 electrode, Environ. Sci. Technol. 43 (2009) 1480–1486.
[51] J.O. Howell, J.M. Goncalves, C. Amatore, L. Klasinc, R.M. Wightman, J.K. Kochi, Electron transfer from aromatic hydrocarbons and their π-complexes with metals. Comparison of the standard oxidation potentials and vertical ionization potentials, J. Am. Chem. Soc. 106 (1984) 3968–3976.
[52] S. Gligorovski, R. Strekowski, S. Barbati, D. Vione, Environmental implications of hydroxyl radicals (•OH), Chem. Rev. 115 (2015) 13051–13092.
[53] D.E. Heard, M.J. Pilling, Measurement of OH and HO_2 in the troposphere, Chem. Rev. 103 (2003) 5163–5198.
[54] L.M. Da Sila, L.A. De Faria, J.F.C. Boodts, Electrochemical ozone production: influence of the supporting electrolyte on kinetics and current efficiency, Electrochim. Acta 48 (2003) 699–709.
[55] H. Herrmann, T. Schaefer, A. Tilgner, S.A. Styler, C. Weller, M. Teich, T. Otto, Tropospheric aqueous-phase chemistry: kinetics, mechanisms, and its coupling to a changing gas phase, Chem. Rev. 115 (2015) 4259–4334.
[56] S. Nehr, B. Bohn, H. Fuchs, A. Hofzumahaus, A. Wahner, HO_2 formation from the OH^+ benzene reaction in the presence of O_2, Phys. Chem. Chem. Phys. 13 (2011) 10699–10708.
[57] J. Iniesta, P.A. Michaud, M. Panizza, G. Cerisola, A. Aldaz, Ch. Comninellis, Electrochemical oxidation of phenol at boron-doped diamond electrode, Electrochim. Acta 46 (2001) 3573.
[58] H. Notsu, I. Yagi, T. Tatsuma, D.A. Tryk, A. Fujishima, Surface carbonyl groups on oxidized diamond electrodes, J. Electroanal. Chem. 492 (2000) 31–37.